Contribution from the Organisch-Chemisches Institut der Universität Heidelberg, Im Neuenheimer Feld 270, 6900 Heidelberg, West Germany

A Green's Function Approach to the Photoelectron Spectra of Transition-Metal Carbonyls

MICHAEL C. BÖHM

Received March 16, 1982

The electronic structures of $Fe(CO)_4H_2$ (**1**), $Mn(CO)_5H$ (**2**), and $Mn(CO)_5CH_3$ (**3**) in the ground state as well as in the cationic hole states are reinvestigated by means of many-body perturbation theory based on the Green's function formalism in the computational framework of a semiempirical INDO Hamiltonian. In the Green's function approach relaxation and correlation effects beyond the Hartree–Fock (HF) picture are taken into account. Various approximations for the self-energy operator are discussed; the validity and the limitations of these models are analyzed. A renormalized model potential for the self-energy part has been employed that allows a straightforward separation into electronic relaxation, the loss of ground-state pair correlation, and the variation of the pair correlation in the cationic hole state. In the numerical calculations for ionization energies in the outer valence region a remarkably good agreement between theory and experiment is encountered. The dependence of the calculated Koopmans defects upon the localization properties of the orbital wave function is rationalized. The INDO calculations on the ground state in the series **1–3** shows that all complexes can be classified as d^6 systems (Fe(2+), Mn(1+)).

1. Introduction

The low-energy photoelectron (PE) spectra of substituted metal pentacarbonyl derviatives $M(CO)_5X$ and of metal tetracarbonyl compounds $M(CO)_4X_2$ have been the subject of various investigations.[1-4] Most of the PE spectra were assigned on the basis of experimental correlation techniques or on the basis of the band intensities as a function of the radiation source (He I/He II).[4] On the other side, there are controversial conclusions derived from purely theoretical approaches. Early semiempirical calculations by Fenske et al.[5] on $Mn(CO)_5X$ derivatives showed a satisfactory agreement between measured and calculated ionization energies if the validity of Koopmans' theorem[6] ($I_{v,j} = -\epsilon_j$) is assumed. In contrast to these findings, ΔSCF ab initio calculations have shown the importance of electronic relaxation, leading to a breakdown of Koopmans' theorem.[2,3] Unfortunately, the ΔSCF calculations in a near double-ζ basis were insufficient to reproduce the experimental sequence of the ionization events.

Significant differences between measured vertical ionization potentials and theoretical values based on the ΔSCF approximation have been encountered in various iron[7] and nickel[8] complexes. Therefore it seems to be of general interest to reinvestigate the PE spectra of the aforementioned transition-metal polycarbonyls by means of theoretical approaches that are beyond the one-particle picture of the Hartree–Fock (HF) model.

Relaxation and correlation effects accompanying the ionization processes can be considered in the framework of many-body perturbation theory based on the Green's function formalism.[9,10] We have applied this method in various transition-metal compounds in combination with an improved INDO Hamiltonian[11] for the assignment of PE data in the outer valence region.[12-14]

In this contribution we have used the Green's function approach for the reinvestigation of the PE spectra of iron tetracarbonyl dihydride ($Fe(CO)_4H_2$ (**1**)) and of the two manganese pentacarbonyl complexes **2** and **3**.

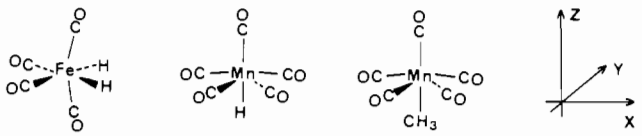

1 **2** **3**

The nonvalidity of Koopmans' theorem in transition-metal compounds has been demonstrated predominantly on the basis of ΔSCF calculations where only relaxation effects are taken into account.[15] Calculations beyond the HF picture are sparse.[16,17] Therefore, the theoretical background of the Green's function method, the necessary limitations, and the relation to the convenient ΔSCF approach are discussed in some detail.

2. Basic Theory

The one-particle Green's function is defined in eq 1.[9,18]

$$G_{ij}(t,t') = -i\langle\Psi_0(N)|\bar{T}[a_i(t)\ a_j(t')]|\Psi_0(N)\rangle \qquad (1)$$

$\langle\Psi_0(N)|$ is the exact ground state of the N-electron system, $\bar{T}$ is the Wick time-ordering operator, and $a_i(t)$, $a_j^+(t')$ the destruction/creation operator in the Heisenberg representation (eq 2 and 3). H is the Hamiltonian of the N electron system.

(1) S. Evans, J. C. Green, A. F. Orchard, and D. W. Turner, *Discuss. Faraday Soc.*, **47**, 112 (1969); D. L. Lichtenberger and R. F. Fenske, *Inorg. Chem.*, **13**, 486 (1974).
(2) M. F. Guest, M. B. Hall, and I. H. Hillier, *Mol. Phys.*, **25**, 629 (1973).
(3) M. F. Guest, B. R. Higginson, D. R. Lloyd, and I. H. Hillier, *J. Chem. Soc., Faraday Trans. 2*, **71**, 902 (1975).
(4) B. R. Higginson, D. R. Lloyd, S. Evans, and A. F. Orchard, *J. Chem. Soc., Faraday Trans. 2*, **71**, 1913 (1975).
(5) R. F. Fenske and R. L. DeKock, *Inorg. Chem.*, **9**, 1053 (1970); D. L. Lichtenberger, A. C. Sarapu, and R. F. Fenske, *ibid.*, **12**, 702 (1973).
(6) T. Koopmans, *Physica (Amsterdam)*, **1**, 104 (1934).
(7) J. A. Connor, L. M. R. Derrick, M. B. Hall, I. H. Hillier, M. F. Guest, R. B. Higginson, and D. R. Lloyd, *Mol. Phys.*, **28**, 1193 (1974); M. B. Hall, I. H. Hillier, J. A. Connor, M. F. Guest, and D. R. Lloyd, *ibid.*, **30**, 839 (1975); J. A. Connor, L. M. R. Derrick, I. H. Hillier, M. F. Guest, and D. R. Lloyd, *ibid.*, **31**, 23 (1976).
(8) M.-M Rohmer and A. Veillard, *J. Chem. Soc., Chem. Commun.*, 250 (1973); M.-M. Rohmer, J. Demuynck, and A. Veillard, *Theor. Chim. Acta*, **36**, 93 (1974).
(9) L. S. Cederbaum and W. Domcke, *Adv. Chem. Phys.*, **36**, 205 (1977).
(10) F. Ecker and G. Hohlneicher, *Theor. Chim. Acta*, **25**, 289 (1972); P. O. Nerbrant, *Int. J. Quantum Chem.*, **9**, 901 (1975); W. von Niessen, L.S. Cederbaum, W. Domcke, and J. Schirmer in "Computational Methods in Chemistry", J. Bargon, Ed., Plenum Press, New York, 1980.
(11) M. C. Böhm and R. Gleiter, *Theor. Chim. Acta*, **59**, 127 (1981).
(12) M. C. Böhm and R. Gleiter, *Theor. Chim. Acta*, **57**, 315 (1980).
(13) M. C. Böhm and R. Gleiter, *J. Comput. Chem.*, **3**, 140 (1982). M. C. Böhm and R. Gleiter, *Chem. Phys.*, **64**, 183 (1982); M. C. Böhm, M. Eckert-Maksič, R. D. Ernst, D. R. Wilson, and R. Gleiter, *J. Am. Chem. Soc.*, **104**, 2699 (1982).
(14) M. C. Böhm, Z. Naturforsch., *A*, **36A**, 1361 (1981); M. C. Böhm, *Theochem*, **87**, 355 (1982).
(15) A. Veillard and J. Demuynck in "Modern Theoretical Chemistry", Vol. 4, H. F. Schaefer, Ed., Plenum Press, New York, 1977.
(16) W. von Niessen and L. S. Cederbaum, *Mol. Phys.*, **43**, 897 (1981).
(17) D. Saddei, H.-J. Freund, and G. Hohlneicher, *Surf. Sci.*, **95**, 527 (1980); D. Saddei, H.-J. Freund, and G. Hohlneicher, *Chem. Phys.*, **55**, 339 (1981).
(18) D. J. Thouless, "The Quantum Mechanics of Many-Body Systems", Academic Press, New York, 1961.

0020-1669/83/1322-0083$01.50/0

$$a_j^+(t) = e^{iHt}a_j^+e^{-iHt} \quad (2)$$

$$a_i(t) = e^{iHt}a_ie^{-iHt} \quad (3)$$

The Fourier-transformed Green's function (4) gives rise to the

$$G_{ij}(\omega) = \int_{-\infty}^{+\infty} G_{ij}(t,t')\, e^{i\omega t}\, dt \quad (4)$$

$$G_{ij}(\omega) = \sum_k \frac{\langle\Psi_0(N)|a_i|\Psi_k(N+1)\rangle\langle\Psi_k(N+1)|a_j^+|\Psi_0(N)\rangle}{\omega + A_k + i\eta} + \sum_k \frac{\langle\Psi_0(N)|a_j^+|\Psi_k(N-1)\rangle\langle\Psi_k(N-1)|a_i|\Psi_0(N)\rangle}{\omega + I_k - i\eta} \quad (5)$$

$$A_k = E_0(N) - E_k(N+1) \quad (6)$$

$$I_k = E_0(N) - E_k(N-1) \quad (7)$$

spectral representation (5), where A_k and I_k are defined in eq 6 and 7. η is a small positive number.[9,19] The Green's function G is completely determined by means of the Dyson (8) or the inverse Dyson equation (9).[20] G^0 is the free Green's function

$$G(\omega) = G^0(\omega) + G^0(\omega)\,\Sigma(\omega)\,G(\omega) \qquad G = G^0 + G^0\Sigma G \quad (8)$$

$$G^{-1} = (G^0)^{-1} - \Sigma = 0 \quad (9)$$

associated with the HF–SCF ansatz as a zeroth-order approximation, and $\Sigma(\omega)$ ($=\Sigma$) is the self-energy part. The vertical ionization energies are related to those ω values for which the matrix of the inverse Dyson equation (9) has eigenvalues equal to zero. In the framework of diagrammatic perturbation theory (8) and (9) can be symbolized by means of (10) and (11).[21] The symbols in eq 10 and 11 can be

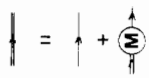

(10)

(11)

extracted from eq 8 and 9. The left sides of the diagrammatic expressions symbolize the Green's functions G and G^{-1}, respectively. The single lines stand for the free Green's function, and Σ is the self-energy operator.

In the case of canonical HF orbitals as a starting point $(G^0)^{-1}$ is simplified to (12), where ϵ is the diagonal matrix of the

$$(G^0)^{-1} = \omega\mathbf{I} - \epsilon \quad (12)$$

canonical HF orbitals and $\mathbf{I}$ the unit matrix. The inverse Dyson equation therefore is given by means of eq 13. $\Sigma(\omega)$

$$G^{-1} = \omega\mathbf{I} - \epsilon - \Sigma(\omega) = 0 \quad (13)$$

can be determined alternatively by a finite approximation to the infinite perturbational series (14) ($\Sigma(\omega)^{(1)}$ vanishes in the

$$\Sigma(\omega) = \Sigma(\omega)^{(2)} + \Sigma(\omega)^{(3)} + \ldots + \Sigma(\omega)^{(\infty)} \quad (14)$$

case of canonical HF orbitals $\{\varphi_i(1)\psi_j(2)\ldots\}$) or via the definition of a two-particle-hole (two-hole-particle) response function R (eq 15) represented by means of the many-body diagram technique.[22,23] R is defined in the form of a Dyson-like equation as a function of the irreducible interaction part X. The lines going down in eq 15 and 16 symbolize hole

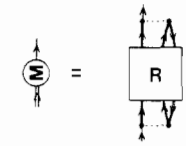

(15)

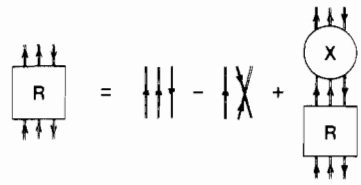

(16)

lines; they are associated to the $N-1$ electron system (cation). The lines going up are called particle lines. The combination of two hole lines and one particle function thus is a model for a cationic state; the wave function is given by determinants of the $N-1$ system in the manifold of particle–hole excitations (single, double, ... excitations). The broken lines in eq 15 are interaction lines that are associated to the two-electron part $(1/r_{12})$ of the molecular Hamiltonian. The crossing of particle and hole lines in eq 16 (exchange interaction) is due to the determinantal nature of the wave function in the HF approximation. The physical meaning of R and X will be clarified in the following equations.

In any case the selected $\Sigma(\omega)$ model should show the same analytical behavior as the exact self-energy operator, which is given as a sum of a constant ω-independent part, $\Sigma(\infty)$, and an ω-dependent part, $M(\omega)$, with simple first-order poles:[22]

$$\Sigma(\omega)_{\text{exact}} = \Sigma(\infty) + M(\omega) \quad (17)$$

To compare the results of a Green's function approach with calculated relaxation energies of a ΔSCF ansatz and to allow a rationalization of the quantum-chemical origin of the nonvalidity of Koopmans' theorem in transition-metal compounds, it is necessary to solve the inverse Dyson equation with an approximation where relaxation and correlation effects can be separated. The ionization process therefore must be described in terms of a simple one-electron wave function picture leading to a decoupling into hole and particle states in eq 12.

In the following, various possibilities for the determination of $\Sigma(\omega)$ according to eq 14 and 15 are discussed. One straightforward way to solve eq 15 is to take into account particle–hole excitations that accompany electron removal (attachment). These processes are called 2h1p (2p1h) excitations (h = hole, p = particle). Within this approximation R (eq 16) is reduced to the recursion (18), where the G lines

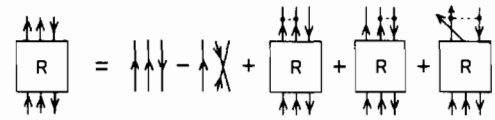

(18)

are given by G^0 lines and the irreducible interaction part X is expressed by its first-order approximation. The broken horizontal lines in eq 18 symbolize the two-electron coupling $(1/r_{12})$ between one-electron wave functions (orbitals) that have been calculated for the electronic ground state (N-electron system). The crossing of the particle and hole lines once again must be traced back to the antisymmetry of the determinantal wave function.

Conveniently R is related to the so-called kernel Γ ($=\Gamma_{lmn,l'm'n'}$),[9,23] which is defined in eq 19 (associated to the

(19) G. Hohlneicher, F. Ecker, and L. S. Cederbaum in "Electron Spectroscopy", D. A. Shirley, Ed., North-Holland, Amsterdam, 1972.
(20) F. J. Dyson, *Phys. Rev.*, **75**, 486 (1949).
(21) P. Nozieres, "Theory of Interacting Fermi Systems", W. A. Benjamin, New York, 1964; E. Economou, "Green's Functions in Quantum Physics", Springer-Verlag, Berlin, 1979; R. D. Mattuck, "Feynman Diagrams in the Many-Body Problem", McGraw-Hill, London, 1967.
(22) J. Schirmer and L. S. Cederbaum, *J. Phys. B*, **11**, 1889 (1978); L. S. Cederbaum, *J. Chem. Phys.*, **62**, 2160 (1975).
(23) C. M. Liegener and U. Scherz, *Theor. Chim. Acta*, **52**, 103 (1979).

$$\Gamma = (\omega\mathbf{I} - K - C)^{-1}\gamma^0 \quad (19)$$

approximation (18)). In the case of the 2p1h set K, C, and γ^0 are given by the equations (20), (21), and (22); the corresponding 2h1p expressions are determined by a modified C term (eq 23) while the K and γ^0 equations are equivalent. ϵ_i in eq 20 is the canonical MO energy of the jth MO, $\delta_{ll'}$ symbolizes the convenient Kronecker δ and the four-index integral $V_{ij[kl]}$ with exchange is defined in eq 24. The one-particle indices are restricted to the conditions given in eq 26 and 27.

$$K_{lmn,l'm'n'} = (-\epsilon_l + \epsilon_m + \epsilon_n)\delta_{ll'}\delta_{mm'}\delta_{nn'} \quad (20)$$

$$C_{lmn,l'm'n'} = -\tfrac{1}{2}\delta_{ll'}V_{mn[m'n']} + \delta_{mm'}V_{ln'[l'n]} + \delta_{nn'}V_{lm'[l'm]} \quad (21)$$

$$\gamma^0{}_{lmn,l'm'n'} = \delta_{ll'}(\delta_{mm'}\delta_{nn'} - \delta_{m'n}\delta_{nm'}) \quad (22)$$

$$C_{lmn,l'm'n'} = \tfrac{1}{2}\delta_{ll'}V_{mn[m'n']} - \delta_{mm'}V_{ln'[l'n]} - \delta_{nn'}V_{lm'[l'm]} \quad (23)$$

$$V_{ij[kl]} = V_{ijkl} - V_{ijlk} \quad (24)$$

$$V_{ijkl} = \langle\varphi_i(1)\ \varphi_j(2)|1/r_{12}|\varphi_k(1)\ \varphi_l(2)\rangle \quad (25)$$

$$n_l\bar{n}_m\bar{n}_n = n_{l'}\bar{n}_{m'}\bar{n}_{n'} = 1 \quad (26)$$

$$\bar{n}_l n_m n_n = \bar{n}_{l'} n_{m'} n_{n'} = 1 \quad (27)$$

Green's function calculations with the kernel (19) are called 2ph-TDA solutions (*T*amm–*D*ancoff *A*pproximation). The matrix dimensions of the original 2ph-TDA ansatz unfortunately are very large, and therefore the solution of the inverse Dyson equation is extremely time consuming even in the case of small- and medium-sized molecules.

In recent semiempirical studies based on the ZDO approximation[17,23,24] additional simplifications have been introduced into (18) and (19). Neglecting the exchange scattering in the irreducible interaction part, one arrives at eq 28 for R

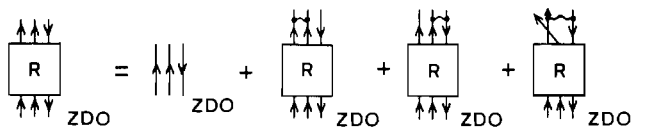

(28)

and eq 29 and 30 for C. In the case of the wiggled interaction lines ($1/r_{12}$) the antisymmetry of the wave function is neglected. This approximation is similar to the neglect of differential overlap in semiempirical models of the ZDO hierarchy (e.g., CNDO, INDO). Thus the infinite summation in the ZDO-adapted response function is performed by means of so-called Feynman graphs characterized by wiggled interaction lines.[25]

$$\text{2p1h:}\quad C_{lmn,l'm'n'} = -\tfrac{1}{2}\delta_{ll'}V_{mn'm'n} + \delta_{mm'}V_{ln'l'n} + \delta_{nn'}V_{lm'l'm} \quad (29)$$

$$\text{2h1p:}\quad C_{lmn,l'm'n'} = -\tfrac{1}{2}\delta_{ll'}V_{mn'm'n} - \delta_{mm'}V_{ln'l'n} - \delta_{nn'}V_{lm'l'm} \quad (30)$$

Within the more elaborate expansion based on (18) a shifted Born collision or diagonal 2p1h TDA for $\Sigma(\omega)$ is given by (31).[9,26] Inspection of eq 31 clearly reveals (energy denominator) that there is no decoupling into hole or particle states

$$\Sigma_{ij}{}^{\text{2p1hTDA}}(\omega) = \tfrac{1}{2}\sum_l\sum_m\sum_n \frac{V_{il[mn]}V_{jl[mn]}(\bar{n}_l n_m n_n + n_l\bar{n}_m\bar{n}_n)}{\omega + \epsilon_l - \epsilon_m - \epsilon_n + (\bar{n}_l n_m n_n - n_l\bar{n}_m\bar{n}_n)\Delta_{lmn}} \quad (31)$$

$$\Delta_{lmn} = \tfrac{1}{2}V_{mn[mn]} - V_{ml[ml]} - V_{nl[nl]} \quad (32)$$

in the Dyson equation. Thus eq 31 prevents the description of ionization processes within a simple one-electron wave function picture and is therefore no suitable tool to link the Green's function method to relaxational approaches (e.g., the ΔSCF formalism). Additionally, important contributions of ground-state correlation energy are neglected in the 2p1h TDA.[22] Nevertheless, (31) is an improvement in comparison to $\Sigma(\omega)^{(2)}$; ionization energies derived with (31) are renormalized with respect to the second-order ansatz leading to the inequivalence relation (33). In the ZDO-adapted simplification, however, eq 34 is fulfilled. The origin of this behavior

$$I_{v_j}{}^{\text{2p1hTDA}} > I_{v_j}{}^{\Sigma(\omega)^{(2)}} \quad (33)$$

$$I_{v_j}{}^{\text{2p1hTDA,ZDO}} < I_{v_j}{}^{\Sigma(\omega)^{(2)}} \quad (34)$$

is recognized in eq 35, where an average Coulomb integral $\bar{V}_{\text{av}}$ has been used in the energy denominator. Due to the sign of $\bar{V}_{\text{av}}$ eq 35 does not lead to a renormalization of the $\Sigma(\omega)^{(2)}$ results, and the calculated ionization energies are lowered once again. Thus neither (18) nor (28) are a suitable framework for a self-energy model with the already discussed properties. In (18) renormalization is taken into account but there is no decoupling into particle and hole states. The opposite is true in the case of (28).

$$\Sigma_{ij}{}^{\text{2p1hTDA,ZDO}}(\omega) = \tfrac{1}{2}\sum_l\sum_m\sum_n \frac{V_{il[mn]}V_{jl[mn]}\bar{n}_l n_m n_n}{\omega + \epsilon_l - \epsilon_m - \epsilon_n - \bar{V}_{\text{av}}} + \tfrac{1}{2}\sum_l\sum_m\sum_n \frac{V_{il[mn]}V_{jl[mn]}n_l\bar{n}_m\bar{n}_n}{\omega + \epsilon_l - \epsilon_m - \epsilon_n + \bar{V}_{\text{av}}} \quad (35)$$

In the case of larger organometallics it is therefore necessary to find an approximation to the infinite perturbational summation (14). The contributions to this expansion can be displayed by means of well-known many-body diagrams;[21] in Figure 1 second-order and third-order contributions to $\Sigma(\omega)$ are shown via a Goldstone representation.[27] The nomenclature corresponds to ref 28. The diagrams in Figure 1 symbolize contributions to the perturbational self-energy expansion. The numerators are given by the multiplication of the various interactions $V_{ij[kl]}$ (e.g., for a second-order diagram, $V_{ij[kl]}{}^2$, for third-order elements, three components). The particle and hole lines in a diagram contribute with ϵ_j to the denominators of the perturbational increments. The hole lines (going down) are associated to the occupied HF orbitals in the N-electron system and the particle lines (going up) to the virtual MO set; the external lines symbolize the spin orbital that has lost the electron in the ionization process. The horizontal interaction lines represent an interaction between four MO's (i, j, k, l) of the HF determinant. The perturbational expressions for the two second-order diagrams therefore simply read (j is the external index ⌒ ionization from the jth MO)

$$\tfrac{1}{2}\sum_a\sum_b\sum_i \frac{V_{ji[ab]}{}^2}{\omega_j + \epsilon_i - \epsilon_a - \epsilon_b}\bar{n}_a\bar{n}_b n_i + \tfrac{1}{2}\sum_a\sum_i\sum_l \frac{V_{ji[al]}{}^2}{\omega_j + \epsilon_a - \epsilon_i - \epsilon_l}\bar{n}_a n_i n_l$$

The signs in the denominators follow from the convenient perturbational rules.[21]

In many-body perturbation theory there exists a hierarchy of tools to derive self-energy models by means of finite contributions to $\Sigma(\omega)$ that are close to the exact self-energy operator. These tools are Kelly's geometric approximation for

(24) S. Biscupič, L. Valko, and V. Kvasnicka, *Theor. Chim. Acta*, **38**, 149 (1975).
(25) R. P. Feynman, "Quantum Electrodynamics", W. A. Benjamin, New York, 1962.
(26) G. Born and Y. Öhrn, *Chem. Phys. Lett.*, **61**, 307 (1979).
(27) J. Goldstone, *Proc. R. Soc. London, Ser. A*, **239**, 267 (1957).
(28) L. S. Cederbaum, *Theor. Chim. Acta*, **31**, 239 (1973); L. S. Cederbaum, *J. Phys. B*, **11**, 1889 (1975).

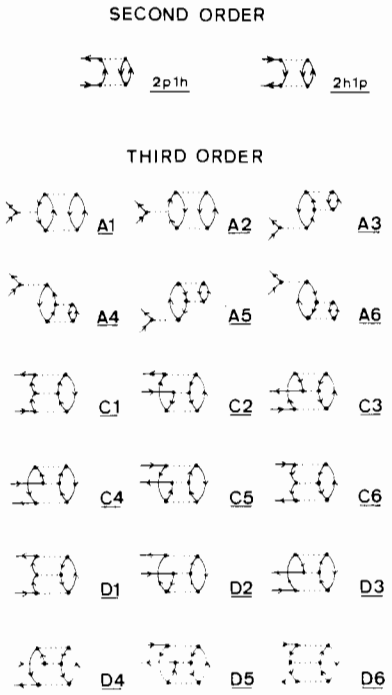

Figure 1. Second- and third-order Goldstone diagrams for the self-energy part.

elements of different order in the $\Sigma(\omega)$ expansion,[29] dressed (renormalized) interactions for interaction, particle, and hole lines, and the dressing of vertices.[21,30] Cederbaum has derived a renormalized self-energy approximation by means of these many-body techniques;[28] the effective self-energy operator in a diagonal approximation is given in eq 36. The associated

$$\Sigma(\omega)_{jj}^{\text{eff}} = \Sigma(\omega)_{jj}^{(2)} + \tfrac{1}{2}(2 \times D_4)_{jj} \qquad (36)$$

diagrams are displayed in Figure 1. This model potential is simple enough to be applicable in medium-sized and larger organometallic compounds. Additionally eq 36 can be decomposed into physically significant relaxation and correlation increments (in contrast to the 2p1h TDA approach), and it has the same analytic structure as eq 17. Therefore we have used (36) as a framework for the calculation of the ionization energies of **1**, **2**, and **3**. It must be mentioned however that the geometric approximation used for the evaluation of (36) is a function of the employed Hamiltonian. This has been verified in a series of calculations where the parameters of a variable semiempirical Hamiltonian have been modified between the model space of an independent electron approximation and a highly correlated valence bond VB operator.[31] Therefore, generally the following inequality between an ab initio ansatz (left-hand side) and a semiempirical MO calculation (right-hand side) with an effective Hamiltonian exists:

$$\left|\frac{\Sigma(\omega)_{jj}^{(n)}}{\Sigma(\omega)_{jj}^{(n+1)}}\right|_{\text{ab initio}} \neq \left|\frac{\Sigma(\omega)_{jj}^{(n)}}{\Sigma(\omega)_{jj}^{(n+1)}}\right|_{\text{semiempirical}}$$

For this difference to be taken into account, a generalized effective renormalized self-energy operator may be defined (eq 37), where k depends on the specific nature of the employed

$$\Sigma(\omega)_{jj}^{\text{eff}} = \Sigma(\omega)_{jj}^{(2)} + k(2 \times D_4)_{jj} \qquad (37)$$

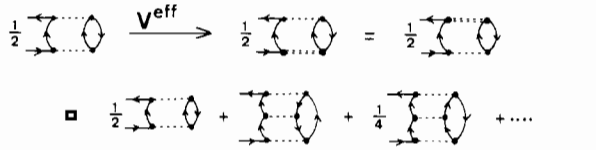

Figure 2. Renormalization of the $V_{ij[kl]}$ points due to the effective interaction V_{eff} verified for the second-order 2p1h diagram.

Hamiltonian. In the present investigation however the original model potential of eq 36 has been used ($k = {}^1/_2$). The self-energy operator in (36) and (37) is already given in a diagonal approximation (eq 38), which is a sufficient model in the outer

$$\Sigma(\omega)_{ij} = \delta_{ij}\Sigma(\omega)_{jj} \qquad (38)$$

valence region; this has been verified both by ab initio[32] and by semiempirical[23,24,33,34] Green's function calculations. Further simplifications used for the determination of the poles in the inverse Dyson equation are described in ref 12. To give some insight into the theoretical formalism leading to eq 36 or 37, we try to rationalize some important key steps of this procedure. Due to its simplicity the dressing (renormalization) of the interaction lines is demonstrated within the self-energy part of the random-phase approximation (RPA). In the electron-gas theory $\Sigma(\omega)$ is given by the sum of the ring diagrams (39).[21] The symbols employed in the following

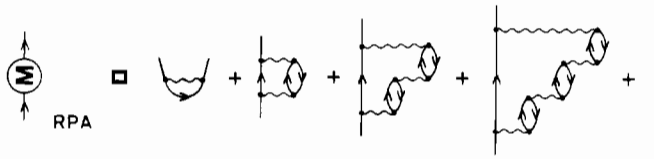

(39)

equations are similar to the diagrammatic expressions used in the foregoing discussion; e.g., the horizontal wiggled lines represent $1/r_{12}$ interactions between one-particle states of the model Hamiltonian, and the vertical lines stand for the free Green's function G^0. If a G^0 line is factored out, the diagrammatic expansion (40) is observed. Therefore the RPA

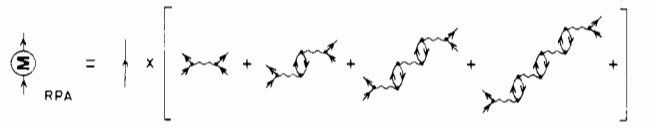

(40)

self-energy operator can be represented by means of (41) and (42), where (42) is the effective interaction potential within the RPA. This concept of an effective interaction V^{eff} of course can be extended beyond the RPA to any expansion for $\Sigma(\omega)$. The defining relations are expressed in eq 43 and 44 in diagrammatic form. V^{eff} is then used to substitute the interaction lines of the $V_{ij[kl]}$ points in the diagrams of Figure 1 with the effective potential (V^{eff}). This is shown in Figure 2. By means of this procedure Cederbaum derived the geometric approximation (36).[28]

In the numerical calculations in section 4 we also used an approximation that has been derived from a self-consistent formalism in the Dyson equation.[21,30] In (10) the G^0 lines are substituted by G lines, which of course are not known; the procedure must be performed up to convergency. This dressing

(29) H. P. Kelly, *Phys. Rev.*, **131**, 684 (1963).
(30) A. L. Fetter and D. L. Walecka, "Quantum Theory of Many-Particle Systems", McGraw-Hill, New York, 1971.
(31) M. C. Böhm, *Ber. Bunsenges. Phys. Chem.*, **86**, 56 (1982); M. C. Böhm, *Chem. Phys.*, **67**, 255 (1982); M. C. Böhm, *Int. J. Quantum Chem.*, in press.
(32) L. S. Cederbaum, G. Hohlneicher, and W. von Niessen, *Chem. Phys. Lett.*, **18**, 503 (1973); L. S. Cederbaum, G. Hohlneicher, and W. von Niessen, *Mol. Phys.*, **26**, 1405 (1973).
(33) P. Lazeratti and R. Zanasi, *Chem. Phys. Lett.*, **42**, 411 (1976); B. Kellerer, L. S. Cederbaum, and G. Hohlneicher, *J. Electron Spectrosc.*, **3**, 107 (1974).
(34) S. Biskupič, L. Valko, and V. Kvasnicka, *Mol. Phys.*, **36**, 1709 (1978).

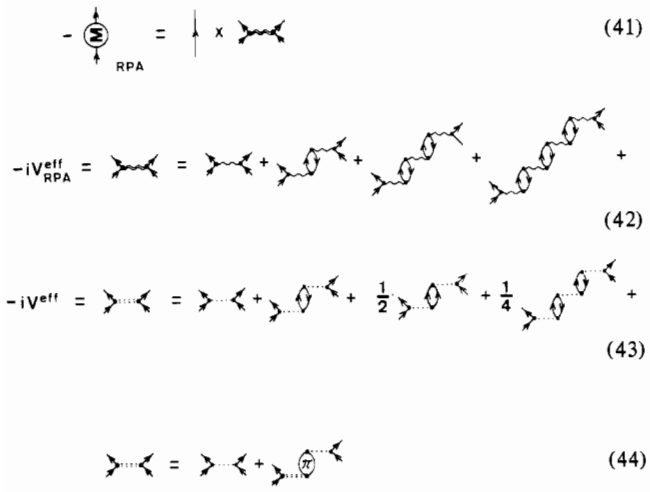

(41)

(42)

(43)

(44)

is shown in eq 45. In a simplified partial self-consistent (PSC)

(45)

approach only the one-electron energies in the energy denominators of $\Sigma(\omega)$ are iterated up to convergence. This algorithm is simple enough to be employed in the case of many-body calculations on larger transition-metal compounds.

3. Separation into Relaxation and Correlation

In this section the self-energy operator is separated into relaxation and correlation increments leading to the net Koopmans defects. Pickup and Goscinski have used the superoperator formalism to develop the Green's function up to second order, leading to a fragmentation into the aforementioned reorganization energies;[35] ref 35 is not based on diagrammatic techniques. With neglect of the ω dependence of the jth ionization potential ($\omega_j \rightarrow \epsilon_j$), eq 46 is valid for I_j (eq

$$-I_j = \epsilon_j + \tfrac{1}{2}\sum_l\sum_m\sum_n \frac{V_{lm[jn]}^2}{\epsilon_j + \epsilon_n - \epsilon_l - \epsilon_m} n_l n_m \bar{n}_n + \tfrac{1}{2}\sum_l\sum_m\sum_n \frac{V_{jl[mn]}^2}{\epsilon_j + \epsilon_l - \epsilon_m - \epsilon_n} n_l \bar{n}_m \bar{n}_n \quad (46)$$

46 is equivalent to a second-order Rayleigh–Schrödinger ansatz). The first sum corresponds to the second-order hole diagram in Figure 1, and the latter sum is associated to the corresponding particle diagram. Equation 46 can be rearranged into (47), where the first two summations have their

$$-I_j = \epsilon_j + \tfrac{1}{2}\sum_l\sum_m \frac{V_{jl[jm]}^2}{\epsilon_m - \epsilon_l} n_l \bar{n}_m + \tfrac{1}{2}\sum_{l}\sum_{m\neq j}\sum_{n} \frac{V_{lm[jn]}^2}{\epsilon_j + \epsilon_n - \epsilon_l - \epsilon_m} n_l n_m \bar{n}_n + \tfrac{1}{2}\sum_l\sum_m\sum_n \frac{V_{jl[mn]}^2}{\epsilon_j + \epsilon_l - \epsilon_m - \epsilon_n} n_l \bar{n}_m \bar{n}_n \quad (47)$$

origin in the hole diagram. The first (double) sum in (47) together with ϵ_j corresponds to the result of a ΔSCF calculation within the HF framework (expanded up to second order):[36]

$$-I_j^{\Delta SCF} = E_0^{(HF)}(N) - E_j^{(HF)}(N-1) = \epsilon_j + \sum_l\sum_m \frac{V_{jl[jm]}^2}{\epsilon_m - \epsilon_l} n_l \bar{n}_m \quad (48)$$

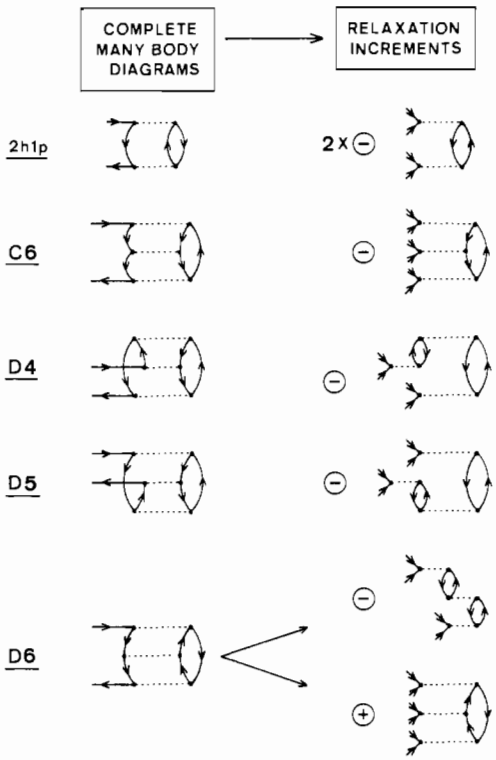

Figure 3. Graphic representation of the projection of the relaxation increments out of the full many-body hole diagrams.

The graphic projection of this relaxation increment out of the second-order hole diagram is[37]

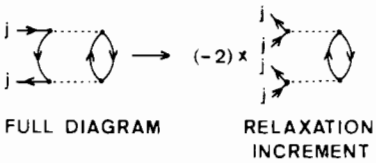

(49)

In the framework of Sinanoğlu's first-order pair-correlation theory[38] also the correlation terms in eq 47 can be traced back to simple physical pictures. The exact energy of the N-electron ground state is defined in eq 50 by means of the HF energy

$$E_0(N) = E_0^{HF}(N) + \tfrac{1}{2}\sum_j\sum_l \epsilon_{jl} \quad (50)$$

$$\epsilon_{jl} = \tfrac{1}{2}\sum_m\sum_n \frac{V_{jl[mn]}^2}{\epsilon_j + \epsilon_l - \epsilon_m - \epsilon_n} n_j n_l \bar{n}_m \bar{n}_n \quad (51)$$

and the additive pairs ϵ_{jl}. The comparison of eq 51 with the third sum of eq 47 clearly shows that this summation corresponds to the loss of ground-state correlation energy due to the ejection of the jth electron. This pair-removal energy (second order) is completely determined by the corresponding particle diagram (see Figure 1). The last correlation element in eq 47 takes into account the variation of the correlation energy in the radical cation as many-body response to the electronic relaxation (pair relaxation). This is seen if ϵ_{lm} for the $N-1$ system is analyzed (eq 52). The last term in eq

$$\epsilon_{lm}^{(N-1)} = \tfrac{1}{2}\sum_n\sum_o \frac{V_{lm[no]}^2}{\epsilon_l + \epsilon_m - \epsilon_n - \epsilon_o} n_l n_m \bar{n}_n \bar{n}_o + \sum_n \frac{V_{lm[jn]}^2}{\epsilon_l + \epsilon_m - \epsilon_j - \epsilon_n} n_l n_m \bar{n}_j \bar{n}_n \quad (52)$$

52 takes into account that j is not occupied in the jth hole state;

(35) B. T. Pickup and O. Goscinski, *Mol. Phys.*, **26**, 1013 (1973).
(36) P. S. Bagus, *Phys. Rev. A*, **139**, 619 (1965); C. M. Moser, R. K. Nesbet, and G. Verhaegen, *Chem. Phys. Lett.*, **12**, 230 (1971).
(37) G. Born, H. A. Kurtz, and Y. Öhrn, *J. Chem. Phys.*, **68**, 74 (1978).
(38) O. Sinanoğlu, *Adv. Chem. Phys.*, **14**, 237 (1969).

the second summation in eq 47 then is the counterpart to this expression.

The second-order particle diagram symbolizes the loss of ground-state pair correlation as a result of the ionization process. In the radical cation the remaining $N - 1$ electrons are reorganized. This reorganization can be divided into a relaxation and a pair-relaxation contribution; both defect increments are part of the second-order hole diagram.

Also in a higher order of perturbation the decomposition into relaxation is possible as there exists a 1:1 correspondence between the $\Sigma(\epsilon_j)_{jj}^{(n)}$ elements of the self-energy part and the correction terms $\Delta E_j(\epsilon_j)_{RS}^{(n)}$ of Rayleigh–Schrödinger perturbation theory ($n \leq 3$)[39] (eq 53–55). $R^{(n)}$ symbolizes a

$$\Delta E_j(\epsilon_j)_{RS}^{(2)} = -\Sigma(\epsilon_j)_{jj}^{(2)} \quad (53)$$

$$\Delta E_j(\epsilon_j)_{RS}^{(3)} = -\Sigma(\epsilon_j)_{jj}^{(3)} \quad (54)$$

$$\Delta E_j(\epsilon_j)_{RS}^{(n)} = R^{(n)} + C2^{(n)} + C1^{(n)} \quad (55)$$

relaxation increment and $C2^{(n)}$ is a pair-relaxation parameter while $C1^{(n)}$ describes a pair-removal correction. $C1^{(n)}$ is always limited to particle diagrams; $R^{(n)}$ and $C2^{(n)}$ are given by hole diagrams. The graphic separation into $R^{(n)}$ and $C2^{(n)}$ for the diagrams in Figure 1 is displayed in Figure 3. Only the set of hole diagrams contains relaxation contributions. The relaxation graph is constructed due to the separation of one or two hole lines, which leads to diagrams where the $V_{ij[kl]}$ points have either none or two external lines (all external lines in Figure 3 correspond to the jth hole state). The sign of the relaxation increments is given by a phase factor that has been derived in ref 37. One relaxation increment is derived from *C6*, *D4*, and *D5*, and two $R^{(3)}$ increments can be projected out of *D6*. The hole diagrams *C4* and *C5* do not contribute to $R^{(3)}$ as no graph with one incoming and one outgoing external line per interaction can be constructed on the basis of the full many-body diagrams.[37] The self-energy model in eq 36 therefore can be symbolized by means of the relaxation and correlation parameters

$$-\Sigma(\omega)_{jj}^{eff} = R^{(2)} + R^{(3)} + C1^{(2)} + C2^{(2)} + C2^{(3)} \quad (56)$$

The explicit formulas for the various elements of this decomposition can be found in the literature.[9,37]

At the end of this section it should be mentioned that the calculated defect components are a function of the employed Hamiltonian. This dependence has been studied in various model calculations with variable electron–electron interaction integrals and one-electron resonance integrals.[31] The calculated deviations from Koopmans' theorem are large in the case of two-electron integrals used in ab initio approaches. If "experimental" quantities are employed, reduced defect increments are predicted. Additionally convergence problems of perturbational expansions are reduced. If the model Hamiltonian simulates a one-electron potential (e.g., the extended Hückel Hamiltonian[40] and Fenske–Hall operator[41]), negligibly small reorganization energies are calculated.[31] A strong coupling between the magnitude and the gradients of the two-electron potential and calculated relaxation and correlation corrections has been found in various mononuclear and binuclear 3d complexes. ΔSCF calculations on ferrocene by means of a recently developed INDO model of Bacon and Zerner with experimental γ integrals[42] lead to Koopmans defects that are much smaller[43] than the relaxation energies

Table I. Orbital Energies, ϵ_i, MO Types, and Composition of the MO's for the Valence Orbitals of **1**, **2**, and **3** According to the INDO Hamiltonian

compd	MO	Γ_i^a	MO type	ϵ_i, eV	% 3d	% H(CH_3)
$Fe(CO)_4H_2$	25	$10a_1$	FeH σ	−11.54	25	38
	24	$6b_2$	Fe $3d_{xz}$	−11.59	74	
	23	$3a_2$	Fe $3d_{yz}$	−12.13	90	
	22	$9a_1$	Fe $3d_{x^2-y^2}$	−12.20	90	
	21	$6b_1$	FeH σ	−12.51	23	43
$Mn(CO)_5H$	29	$2b_2$	Mn $3d_{xy}$	−11.29	80	
	27/28	7e	Mn $3d_{xz}/3d_{yz}$	−11.31	81	
	26	$8a_1$	MnH σ	−11.94	20	43
$Mn(CO)_5CH_3$	32	$9a_1$	Mn C_{CH_3} σ	−11.08	20	51
	31	$2b_2$	Mn $3d_{xy}$	−11.27	79	
	29/30	8e	Mn $3d_{xz}/3d_{yz}$	−11.33	83	

[a] The numbering scheme of the irreducible representations corresponds to the configuration of the valence electrons.

in ab initio studies[44] and that are smaller than the corrections predicted with the present INDO model.[45] Furthermore, this problem is closely related to observed instabilities of the HF solution in ab initio calculations (symmetry violations) that are not found in approximate studies.[46] The quantum-chemical origin for all these phenomena is the screening of the two-electron potential in model Hamiltonians that are not based on HF ab initio integrals. In a recent study this mutual dependence (the validity of the HF picture and the analytic form of the two-electron potential) has been studied in great detail in the case of binuclear Ni complexes.[47]

4. Ground-State Properties

To simplify the interpretation of the Green's function calculations on the cationic hole states, it is necessary to analyze the ground-state properties as derived with the semiempirical INDO Hamiltonian.[11]

$Fe(CO)_4H_2$ belongs to the point group C_{2v} with the H ligands on the equatorial positions.[48] The $C_{ax}FeC_{ax}$ angle amounts to 148.5° with a bent deformation into the direction of the H atoms. The electronic structure of **1** therefore must correspond to a distorted octahedron with three occupied MO's of predominant Fe 3d character that are related to the triply degenerate t_{2g} set under O_h symmetry.

The two manganese pentacarbonyl complexes **2** and **3** are representatives of a series of $M(CO)_5X$ compounds that have been of great interest to experimental[1,4,49] and theoretical[2,5] workers. In both Mn complexes the central atom shows a distorted-octahedral coordination as the equatorial CO ligands are displaced into the direction of the axial ligand X (X = H, CH_3). In **2** a $C_{ax}MnC_{eq}$ angle α of 97° has been determined;[47,50] in **3** α is 95°:[51]

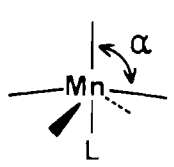

(39) A. J. Hernandez and P. W. Langhoff, *Chem. Phys. Lett.*, **49**, 127 (1977).
(40) R. Hoffmann, *J. Chem. Phys.*, **39**, 1397 (1963); R. Hoffmann and W. N. Lipscomb, *J. Chem. Phys.*, **36**, 2179, 3489 (1962).
(41) M. B. Hall and R. F. Fenske, *Inorg. Chem.*, **11**, 768 (1972).
(42) A. D. Bacon and M. C. Zerner, *Theor. Chim. Acta*, **53**, 589 (1979).
(43) M. C. Zerner, G. H. Loew, R. F. Kirchner, and U. T. Mueller-Westerhoff, *J. Am. Chem. Soc.*, **102**, 589 (1980).
(44) M.-M. Coutière, J. Demuynck, and A. Veillard, *Theor. Chim. Acta*, **27**, 281 (1972); P. S. Bagus, U. I. Wahlgren, and J. Almlöf, *J. Chem. Phys.*, **64**, 2324 (1976).
(45) M. C. Böhm, R. Gleiter, and F. Delgado-Pena, *Inorg. Chem.*, **19**, 1081 (1980).
(46) B. E. Bursten, J. R. Jensen, D. J. Gordon, P. M. Treichel, and R. F. Fenske, *J. Am. Chem. Soc.*, **103**, 5226 (1981).
(47) M. C. Böhm, submitted for publication in *Int. J. Quantum Chem.*
(48) E. A. McNeill and F. R. Scholer, *J. Am. Chem. Soc.*, **99**, 6243 (1977).
(49) (a) F. A. Cotton and R. M. Wing, *J. Organomet. Chem.*, **9**, 511 (1967); (b) H. B. Gray, E. Billig, A. Wojcicki, and M. Farona, *Can. J. Chem.*, **41**, 1281 (1963); (c) S. Cradock, E. A. V. Ebsworth, and A. Robertson, *J. Chem. Soc., Dalton Trans.* 22 (1973).
(50) S. J. LaPlaca, W. C. Hamilton, J. A. Ibers, and A. Davison, *Inorg. Chem.*, **8**, 1928 (1969).

Table II. Net Charges in the Series 1-3 According to the Present INDO Model

compd	3d center	C_{ax}	O_{ax}	C_{eq}	O_{eq}	C_{CH_3}	$H_{CH_3}(3)$
$Fe(CO)_4H_2$	0.228+	0.217+	0.194–	0.191+	0.177–		0.148–
$Mn(CO)_5H$	0.141–	0.211+	0.183–	0.265+	0.202–		0.148–
$Mn(CO)_5CH_3$	0.165–	0.214+	0.184–	0.280+	0.218–	0.480–	0.117+

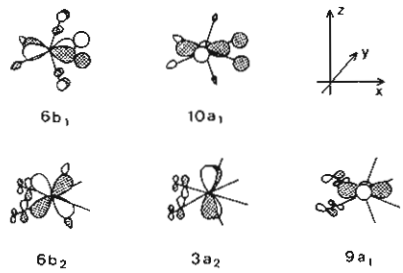

Figure 4. Qualitative representation of the outer valence orbitals of 1.

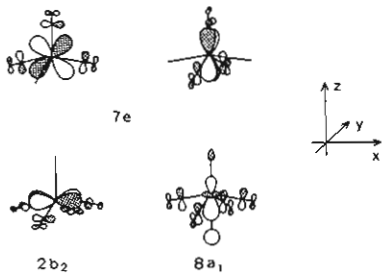

Figure 5. Qualitative representation of the outer valence orbitals of 2 and 3.

Qualitative explanations for these preferences have been worked out in detail by Elian and Hoffmann.[52] In Table I the INDO MO energies for the outer valence orbitals of **1**, **2**, and **3** are summarized. Schematic representations of the corresponding orbitals are given in Figures 4 and 5. In **1** five complex MO's are separated by about 3 eV from the CO π and σ linear combinations. Table I shows that the two FeH σ MO's at −11.54 and −12.51 eV are separated by three orbitals predominantly localized at the 3d center. The two FeH σ linear combinations have Fe 3d amplitudes of 25% (MO 25) and 23% (MO 21), respectively. In the case of the "Fe 3d" orbitals ($6b_2$, $3a_2$, and $9a_1$) $3a_2$ and $9a_1$ show the most pronounced localization at the transition-metal center (90%). A significant metal–ligand coupling is encountered in $6b_2$, where the axial σ CO functions are able to mix with $3d_{xz}$ due to the bending motion of the two CO ligands. The Fe 3d amplitude in this MO therefore is reduced to 74%. The valence orbitals of the metal tetracarbonyl fragment have been analyzed in more detail by Burdett[53] and by Elian and Hoffmann.[52]

In the two manganese complexes **2** and **3** the Mn 3d orbitals split into $a_1(3d_{z^2})$, $b_1(3d_{x^2-y^2})$, and $b_2(3d_{xy})$ and a degenerate $e(3d_{xz}, 3d_{yz})$ combination; in both pentacarbonyls the point group C_{4v} is used to label the MO's. In a d^6 complex (Mn(1+)) b_2 and e are occupied while a_1 and b_1 belong to the virtual Fermi sea. Thus b_2/e combinations are related to t_{2g} of an unperturbed octahedron while a_1/b_1 combinations correlate with the doubly degenerate e_g combination in the case of O_h symmetry.

In the hydride complex **2** INDO predicts the following ground-state sequence for the outer valence orbitals: $(8a_1)^2(7e)^4(2b_2)^2$. The Mn 3d combinations are on top of the MnH σ bond. The gap between $2b_2$ and 7e is only 0.02 eV; the MnH σ linear combination is stabilized by about 0.62 eV from the Mn 3d functions. The CO valence orbitals are separated by more than 2.5 eV from these MO's. $2b_2$ and 7e show comparable Mn 3d amplitudes (about 80%). In analogy to the case for **1** significant CO contributions are predicted for the $8a_1$ MnH σ combination. The 1s contribution of H amounts to 43%, and the Mn 3d(:$3d_{z^2}$) admixture is 20%.

In the case of the methyl complex **3** INDO predicts for the ground state a switch of the MO sequence Mn 3d/MnX σ. Here $9a_1$ ($MnCH_3$ σ) is predicted on top of the Mn 3d linear combinations $2b_2$/8e. $9a_1$, $2b_2$, and 8e are found in an energy interval of only 0.25 eV (−11.08, −11.27, −11.33 eV). The compositions of the orbital wave functions are similar to those of **2**. The present INDO calculations on **2** and **3** differ from ab initio results of Guest et al.[2] insofar as in the ab inito framework a_1 is always predicted on top of b_2/e.

In Table II we have summarized the net charges of **1**–**3**.[54] The heteroligands show in any case a charge excess. In **1** a H net charge of −0.148 e is predicted; the same value is derived in **2**. This occupation pattern is in line with experimentally determined proton shifts that are comparable with a net charge between 0.1– and 0.4–.[55]

Chart I

assignment	I_{vj}^{exptl}, eV	$I_{vj}^{\Delta SCF}$, eV: ab initio	$I_{vj}^{\Delta SCF}$, eV: CNDO
$2A_1$	9.65	...	7.0
$2B_2$		9.2	7.0
$2A_2$		9.4	7.1
$2B_1$	10.95	9.1	7.3
$2A_1$	11.30		11.3

5. Calculation of the Ionization Energies

In the following we want to restrict our discussion to ionization events in the lower energy region as the CO bands belong to a broad band system without distinct maxima. $Fe(CO)_4H_2$ shows two bands in the outer valence region below 14 eV.[3] The first peak has its maximum at 9.65 eV, and the second band is highly unsymmetric with a maximum at 10.95 eV and a high-energy shoulder at 11.30 eV. These IP's are separated by more than 3 eV from the CO ionization events. On the basis of the comparison with PE spectra of related iron carbonyl complexes ($Fe(CO)_5$/$Fe(CO)_4C_2H_4$,[56] halogenated $Fe(CO)_4$ ethylene derivatives,[57] iron tetracarbonyl carbene complexes,[58] and iron tricarbonyl species[7]) it is clear that the first band of **1** has to be assigned to the three Fe 3d linear combinations $6b_2(3d_{xz})$, $3a_2(3d_{yz})$, and $9a_1(3d_{x^2-y^2})$ while the second band must correspond to the FeH σ linear combinations. This assignment is supported due to the ionization sequence in the series $Fe(CO)_4H_2$,[3] $Co(CO)_4H$,[49] and $Mn(CO)_5H$.[1-3]

The ionization sequence of **1** could be reproduced satisfactorically neither by ΔSCF ab initio calculations of near double-ζ quality[3] nor by ΔSCF CNDO calculations based on a recent ZDO extension to the 3d series[59] (Chart I). We have

(51) H. M. Seip and R. Seip, *Acta Chem. Scand.*, **24**, 3431 (1970).
(52) M. Elian and R. Hoffmann, *Inorg. Chem.*, **14**, 1058 (1975).
(53) J. K. Burdett, *J. Chem. Soc., Faraday Trans. 2*, **70**, 1599 (1974).
(54) R. S. Mulliken, *J. Chem. Phys.*, **23**, 1833, 2343 (1955).
(55) L. L. Lohr and W. N. Lipscomb, *Inorg. Chem.*, **3**, 22 (1964).
(56) H. van Dam and A. Oskam, *J. Electron Spectrosc.*, **16**, 307 (1979); H. van Dam and A. Oskam, *ibid.*, **17**, 357 (1979).
(57) E. J. Baerends, C. Oudshoorn, and A. Oskam, *J. Electron Spectrosc.*, **6**, 259 (1975).
(58) M. C. Böhm, J. Daub, R. Gleiter, P. Hofmann, M. F. Lappert, and K. Öfele, *Chem. Ber.*, **113**, 3629 (1980).

Table III. Comparison between the Measured Vertical Ionization Potentials ($I_{v,j}^{exptl}$) of $Fe(CO)_4H_2$ and Those Calculated[a]

peak	Γ_j	$I_{v,j}^{K}$	$I_{v,j}^{K} + \Sigma^{(2)}$	$I_{v,j}^{K} + \Sigma^{eff}$	$I_{v,j}^{exptl}$
1	$9a_1$	12.20	8.31	9.36	
	$6b_2$	11.59	8.58	9.36	9.65
	$3a_2$	12.13	8.54	9.48	
2	$10a_1$	11.54	10.50	10.73	10.95
	$6b_1$	12.51	11.50	11.71	11.30 sh

[a] $I_{v,j}^{K}$ is based on the validity of Koopmans' theorem. $I_{v,j}^{K} + \Sigma^{(2)}$ has been derived by means of the inverse Dyson equation with the second-order self-energy approximation; $I_{v,j}^{K} + \Sigma^{eff}$ corresponds to the renormalized ansatz. All values are in eV; sh = shoulder.

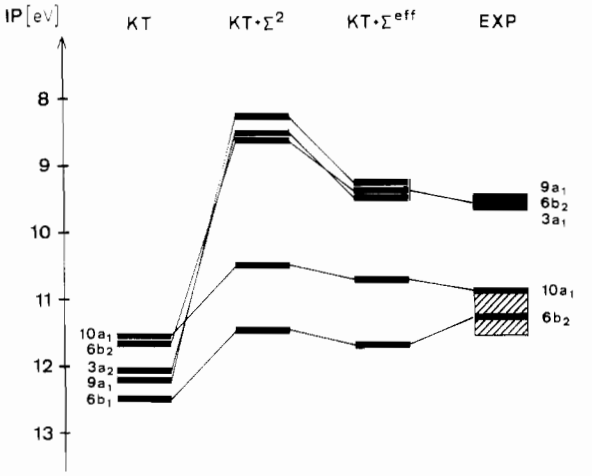

Figure 6. Comparison between the measured vertical ionization potentials (EXP) of $Fe(CO)_4H_2$ and those calculated with the assumption of the validity of Koopmans' theorem (KT) and with the inverse Dyson equation. KT + $\Sigma^{(2)}$ corresponds to a second-order approximation for the self-energy part; KT + Σ^{eff} symbolizes the renormalized ansatz.

compared the ΔSCF results (ab initio and semiempirical CNDO approach) with measured ionization energies although it is difficult to relate molecular properties or the MO picture with these calculations. Nevertheless we felt that this opposition shows impressively the shortcomings of the ΔSCF model independent of the nature of the model Hamiltonian.

The INDO-based Green's function results are summarized in Table III and Figure 6. In the determination of the self-energy part 12 hole and 10 particle states have been considered; PSC effects were negligible (modifications smaller than 0.05 eV). It is clearly seen that the measured ionization energies are reproduced with high accuracy. For the Fe 3d MO's $9a_1$, $6b_2$, and $3a_2$ IP's of 9.36, 9.36, and 9.48 eV, respectively, are predicted. The calculated center of gravity differs only 0.25 eV from the experimental band maximum. Also in the case of the two FeH σ orbitals the close correspondence between theory and experiment is recognized; the separation between the $10a_1$ and the $6b_2$ ionizations is slightly overestimated. The calculated center of gravity (11.33 eV) differs by only 0.11 eV from the experimental center of gravity (11.22 eV).

Table III and Figure 6 also display the importance of renormalization in the case of the strongly localized MO's. Second-order defects of 3.89 ($9a_1$), 3.01 ($6b_2$), and 3.59 eV ($3a_2$) are calculated by means of the INDO ansatz. The corresponding third-order corrections are −1.05 ($9a_1$), −0.78 ($6b_2$), and −0.94 eV ($3a_2$). The net defects for the Fe 3d

(59) D. W. Clack, N. S. Hush, and Y. R. Yandle, *J. Chem. Phys.*, **57**, 3503 (1972).

Chart II

	assignment	$I_{v,j}^{exptl}$, eV	$I_{v,j}^{ΔSCF}$, eV ab initio	CNDO
$Mn(CO)_5H$	^2E	8.85	8.2	4.2
	$^2B_2$	9.14	8.6	4.3
	$^1A_1$	10.55	8.4	8.1
$Mn(CO)_5CH_3$	^2E	8.65	8.0	4.4
	$^2B_2$	9.12	8.6	4.5
	$^2A_1$	9.49	7.5	9.0

Table IV. Comparison between the Measured Vertical Ionization Potentials of $Mn(CO)_5H$ and Those Calculated[a]

peak	Γ_j	$I_{v,j}^{K}$	$I_{v,j}^{K} + \Sigma^{(2)}$	$I_{v,j}^{K} + \Sigma^{eff}$	$I_{v,j}^{K} + \Sigma^{eff}$ + PSC	$I_{v,j}^{exptl}$
1	7e	11.31	7.72	8.86	8.87	8.85
2	$2b_2$	11.29	8.46	9.35	9.16	9.14
3	$8a_1$	11.94	10.62	10.96	10.95	10.55

[a] See the legend to Table III. $I_{v,j}^{K} + \Sigma^{eff}$ + PSC corresponds to the iteration of the inverse Dyson equation.

ionization events therefore span a range between 2.23 and 2.84 eV. For the FeH σ linear combinations Koopmans defects smaller than 1 eV are predicted.

The PE data of **1** suggest the following simplified description for the electronic structure of the Fe complex: $Fe(CO)_4^{2+}$ and $2H^-$, which is formally a d^6 system. In analogy to the case for various Fe tricarbonyl complexes with butadiene, trimethylenemethane, and cyclobutadiene[7] all Fe 3d ionization events occur as a single band, indicating that the corresponding electrons in the cationic hole states are similar to those of their t_{2g} parent of an unperturbed octahedron. In the ground state of **1** an energy gap of 0.6 eV is predicted for the Fe 3d valence orbitals; the calculated ionization energies with the inclusion of correlation and relaxation are separated by only 0.12 eV.

The low-energy PE spectrum of **2** shows two band systems on the low-energy side of the carbonyl ionization events starting at 13.40 eV.[49c] The first band has two distinct maxima at 8.85 and 9.14 eV. The first component with the larger cross section must be assigned to the degenerate 7e ($3d_{xz}/3d_{yz}$) linear combination and the second maximum to an ionization out of $2b_2$ ($3d_{xy}$). The MnH σ ionization is found at 10.55 eV. This assignment has been derived on the basis of experimental correlation techniques with related transition-metal carbonyls.[49c]

The Mn $3d_{xy}$ ($2b_2$) and the MnX σ ionization potentials of **3** collapse into a common band system. The $2b_2$ maximum is found at 9.12 eV, and the $9a_1$ ionization leads to a high-energy shoulder at 9.49 eV. The first IP of **3** out of 8e is encountered at 8.65 eV. Once again ΔSCF calculations with the ab initio basis or in the CNDO framework did not reproduce satisfactorily the experimental ionization sequence as well as the magnitude of the IP's[3] (Chart II). The Green's function results for **2** are summarized in Table IV and Figure 7. The perturbational summation covers 14 hole and 12 particle states; additionally the PSC iteration has been employed. Inspection of Table IV and Figure 7 demonstrates that the Green's function formalism (Σ^{eff} + PSC) reproduces the Mn 3d ionization potentials with an accuracy that is within the experimental error. In the case of the degenerate 7e combination 8.87 eV (theory) must be compared with 8.85 eV (experiment). In the case of $2b_2$ the corresponding values are 9.16 and 9.14 eV. The agreement is less quantitative for the MnH σ ionization; the measured IP is 0.40 eV smaller than the calculated one.

Remarkable deviations from Koopmans' therorem are calculated for the ionization events out of strongly localized Mn 3d orbitals. For 7e a second-order defect of 3.59 eV is

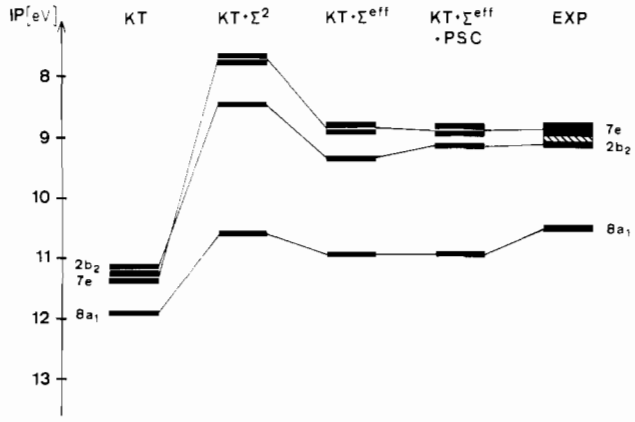

Figure 7. Comparison between measured vertical ionization potentials of $Mn(CO)_5H$ and those calculated (see the legend for Figure 6). KT + Σ^{eff} + PSC represents the renormalized self-energy odel with partial self-consistent iterations.

Table V. Comparison between the Measured Vertical Ionization Potentials of $Mn(CO)_5CH_3$ and Those Calculated[a]

peak	Γ_j	$I_{v,j}^K$	$I_{v,j}^K + \Sigma^{(2)}$	$I_{v,j}^K + \Sigma^{eff}$	$I_{v,j}^{exptl}$
1	8e	11.33	7.75	8.89	8.65
	$2b_2$	11.27	8.28	9.13	9.12
2	$9a_1$	11.08	10.40	10.58	9.49 sh

[a] See the legend to Table III.

predicted. In the case of $2b_2$ only a reorganization increment of 2.83 eV is encountered. The third-order renormalization for these two MO's are −1.14 and −0.89 eV, respectively. The PSC iteration lowers the IP of $2b_2$ by 0.19 eV while 7e is nearly constant. The net defects within the present INDO Hamiltonian thus amount to 2.44 (7e) and 2.13 eV ($2b_2$). The reorganization energies in $8a_1$ are less pronounced. The second-order defect of 1.32 eV is reduced by 0.33 eV due to the combined effects of Σ^{eff} and PSC.

The Green's function results for **3** are summarized in Table V and Figure 8. In the perturbational summation 14 hole-states and 12 particle functions have been employed. With the exception of $9a_1$, once again an almost perfect agreement between the experimental values and the calculated IP's is encountered. For 8e 8.89 (theory) and 8.65 eV (experiment) must be correlated (in the case of the $3d_{xy}$ combination: 9.13 and 9.12 eV). Only for the $MnCH_3$ σ ionization is a difference of 1.09 eV between the calculated and the measured IP found.

The PE spectra of **2** and **3** differ significantly from the PE data of the iron complex **1**. The Fe 3d ionization events in **1** ($9a_1$, $3a_2$, and $6b_2$) are degenerate and therefore have a close correspondence to the t_{2g} set of an octahedron. In **2** and **3** the Mn 3d functions of E and B symmetry are also related to t_{2g} in the point group O_h. In contrast to the case for **1** separated PE bands are found while the energy gap in the electronic ground state is negligble.

6. Fragmentation of the Net Reorganization Energies into Correlation and Relaxation Contributions

In section 3 it has been demonstrated that the net Koopmans defects that are calculated in the diagonal approximation for the self-energy operator can be fragmented into relaxation and correlation increments. In Table VI we have summarized this decomposition for the outer valence orbitals of $Mn(CO)_5H$; the results for **3** are similar, and thus they are not presented in detail. The fragmentation in the case of **1** as well an analysis of reorganization energies in various other iron complexes is given in a separate contribution.[60] A graphic display of the

(60) M. C. Böhm, *Theor. Chim. Acta*, **61**, 539 (1982).

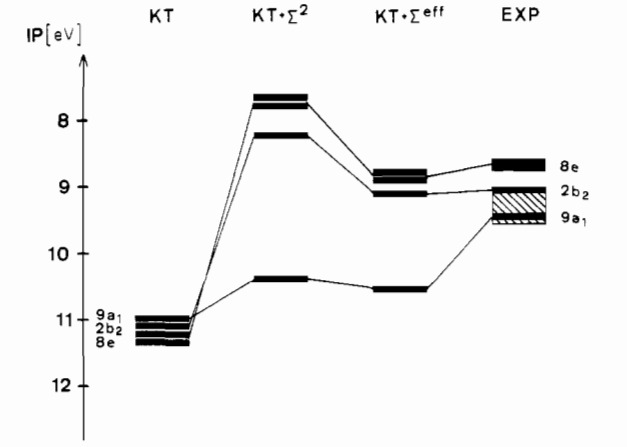

Figure 8. Comparison between measured vertical ionization potentials of $Mn(CO)_5CH_3$ and those calculated (see the legend for Figure 6).

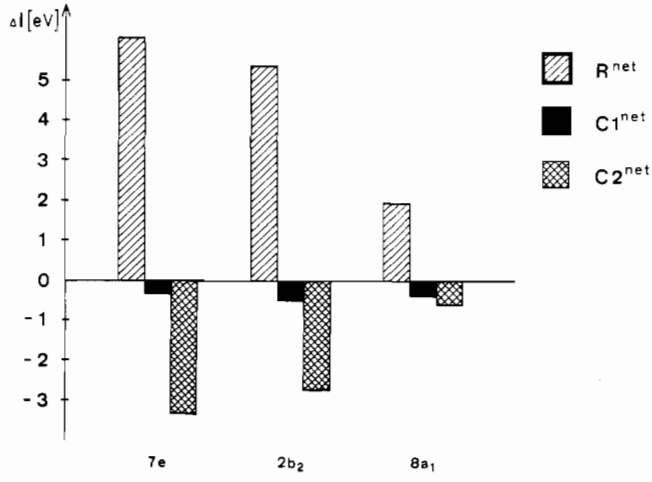

Figure 9. Decomposition of the net Koopmans defects of $Mn(CO)_5H$ into relaxation (R), pair-removal ($C1$), and pair-relaxation ($C2$) increments according to the present INDO model.

theoretical findings for **2** is shown in Figure 9.

The net defects ΔI_j are separated into second- ($R^{(2)}$) and third-($R^{(3)}$) order relaxation components and into a second-order ($C1^{(2)}$) pair-removal increment as well as into second- and third-order contributions for the pair-relaxation energy ($C2^{(2)}$, $C2^{(3)}$). The physical meaning of these contributions has been discussed in section 3.

It is seen that the relaxation increments are the predominant contributions to ΔI_j for the two strongly localized Mn 3d linear combinations. The net lowering of I_{vj}^K due to R^{net} amounts to 6.07 (7e) and 5.36 eV ($2b_2$), respectively. In both one-electron functions there are pronounced renormalization corrections (−1.15, −0.95 eV). The magnitude of the pair-relaxation energies however demonstrates that it cannot be expected to reproduce PE spectra of transition-metal compounds by means of purely relaxational procedures. The modification of the pair-correlation energy in the cationic hole state is too large to be neglected.

In **2** net pair-relaxation contributions of −3.32 (7e) and −2.74 eV ($2b_2$) are calculated that act into the opposite direction from that of the electronic relaxation. While R^{net} has a pronounced lowering effect for the calculated ionization energies, $C2^{net}$ partially compensates the magnitude of the net defects. In any case R^{net} dominates $C2^{net}$. In the $8a_1$ MnH σ combination both contributions are significantly reduced; here a total relaxation energy of 1.92 eV is calculated while $C2^{net}$ amounts to −0.57 eV. In comparison to the case for 7e and $2b_2$ pair-correlation modifications in the $N-1$ system are less important.

Table VI. Decomposition of the Calculated Koopmans Defects ΔI_j in $Mn(CO)_5H$ into Relaxation, Pair-Removal, and Pair-Relaxation Contributions (All Values in eV)

Γ_j	ΔI_j	$R^{(2)}$	$R^{(3)}$	R^{net}	$C1^{(2)} = C1^{net}$	$C2^{(2)}$	$C2^{(3)}$	$C2^{net}$
7e	2.45	7.22	−1.15	6.07	−0.30	−3.34	0.02	−3.32
$2b_2$	2.13	6.31	−0.95	5.36	−0.49	−2.99	0.25	−2.74
$8a_1$	0.99	2.19	−0.27	1.92	−0.36	−0.52	−0.05	−0.57

The loss of ground-state pair correlation ($=C1^{(2)} = C1^{net}$ in the framework of the renormalized self-energy part) is nearly independent of the nature of the orbital wave function and is small in comparison to R^{net} and $C2^{net}$. $C1^{net}$ has a raising effect, which lies between −0.3 and −0.5 eV.

The fragmentation scheme employed in Table VI clearly demonstrates that calculated IP's in the ΔSCF approximation are too small if a Hamiltonian has been employed with a basis set near the HF limit. This failure of purely relaxational methods has been demonstrated in a series of ΔSCF ab initio calculations with large basis sets.[8] The agreement between measured IP's and ΔSCF ab initio calculations far from the HF limit is therefore a rather fortuitous one as deviations from the HF limit and the neglected $C1^{net}/C2^{net}$ contributions nearly compensate each other. In any case it has been demonstrated that theoretical methods beyond the HF picture are necessary to reproduce PE spectra of transition-metal compounds if model Hamiltonians with a two-electron part are used in the calculations (ab initio or semiempirical models). Of course the whole argumentation is invalid in the case of one-electron operators (e.g., the extended Hückel, Fenske–Hall Hamiltonian), where the $1/r_{12}$ term is included in an effective operator that is independent of the coordinates of two electrons.

The absolute numbers of the relaxation and correlation increments determined in the present study are a function of the analytic form of the employed Hamiltonian. The general findings (e.g., the imbalance of relaxation and pair relaxation and reduced $C1^{net}$ corrections in comparison to those for $R1^{net}/C2^{net}$), however, are independent of the actual parameterization and are encountered in all approaches with $1/r_{12}$ elements in the molecular Hamiltonian. This aspect has been discussed in greater detail in ref 31.

7. Conclusion

The low-energy PE spectra of the carbonyl complexes **1**–**3** have been investigated by means of many-body perturbation theory based on the Green's function formalism. The computational framework was an improved INDO model. In contrast to the case for published ΔSCF calculations (ab initio and semiempirical CNDO procedures) ionization energies close to the measured data have been derived. We have used a perturbational expansion where the net reorganization energies can be decomposed into relaxation and correlation increments with definite physical information. This fragmentation has clearly demonstrated that relaxation and correlation effects must be taken into account if Hamiltonians with the $1/r_{12}$ potential are employed in model calculations. The cancellation of relaxation and correlation that is found in strongly delocalized MO's is not observed in 3d complexes with localized molecular orbitals. The success of one-electron calculations of the Fenske–Hall type must be traced back to the fact that this imbalance is removed if the $1/r_{12}$ part has been removed from the molecular Hamiltonian (one-electron operator). The theoretical shortcoming of the latter method, on the other hand, is the necessity of using scaling constants for some bands in the PE spectrum.[41]

The present Green's function calculations need about 30 min of CPU time on an IBM 370/168 computer; the time-consuming step in a semiempirical calculation of course is the calculation of the four-index integrals V_{ijkl}. The large advantage of approaches based on ground-state wave functions lies in the fact that SCF difficulties in the iterations on the deeper cationic states or variational collapses encountered in ΔSCF calculations[61] are avoided.

The numerical results derived for **1**, **2**, and **3** have demonstrated that relaxation and pair relaxation in the cationic hole state depend critically on the localization properties of the orbital wave function. R^{net} and $C2^{net}$ are the two most important increments leading to the breakdown of Koopmans' theorem in transition-metal compounds. The loss of ground-state pair correlation due to the removal of one electron is small in comparison to R^{net} and $C2^{net}$.

Acknowledgment. This work has been supported by the Stifung Volkswagenwerk. The assistance of Mrs. H. Wellnitz and Mrs. I. Grimmer in the preparation of the manuscript is gratefully acknowledged.

Registry No. **1**, 22763-20-8; **2**, 16972-33-1; **3**, 13601-24-6; $[Fe(CO)_4H_2]^+$, 83221-18-5; $[Mn(CO)_5H]^+$, 83221-19-6; $[Mn(CO)_5CH_3]^+$, 83221-20-9.

(61) M. E. Schwartz, *Chem. Phys. Lett.*, **5**, 50 (1977); M. Hehenberger, *ibid.*, **46**, 117 (1977); D. Firsht and B. T. Pickup, *Int. J. Quantum Chem.*, **12**, 765 (1977); M. Doran, I. H. Hillier, E. A. Seddon, K. R. Seddon, V. H. Thomas, and M. F. Guest, *Chem. Phys. Lett.*, *63*, 612 (1979).